J. Micromech. Microeng. **9** (1999) 236–244. Printed in the UK PII: S0960-1317(99)00878-5

On the buckling behavior of micromachined beams

Weileun Fang, Chun-Hsien Lee and Hsin-Hua Hu

Power Mechanical Engineering Department, National Tsing Hwa University, Hsinchu, Taiwan

Received 12 January 1999

Abstract. Thin film materials are normally under residual stresses as a result of fabrication processes. Unlike microelectronics devices, a micromechanical structure is no longer constrained by its underlying silicon substrate after anisotropic etch undercutting; therefore, residual stresses may result in the bending and buckling of a micromechanical structure. The buckling behavior has been exploited to measure the residual stresses of thin films. This characteristic can also be applied to fabricate out-of-plane three-dimensional micromechanical structures if their deflections are controllable. The buckling of a microbridge is difficult to predict since it is strongly dominated by its fabrication processes and boundary conditions. Currently the information regarding the buckling of micromachined structures is still not complete. The application of the buckling behavior is therefore limited. In this research, the effects of boundary conditions and gradient residual stresses on the buckling behavior of microbridges were studied using analytical and experimental approaches. The variations of the buckling amplitude orientations with the thickness and length of the microbridges were obtained; therefore, the buckling behavior can be predicted and then exploited to fabricate useful micromechanical structures. The potential application of this research lies in preventing the leakage of the microvalves.

1. Introduction

As the result of fabrication processes, thin film materials are normally under residual stresses [1]. The residual stresses may lead to unwanted deformation, such as bending, buckling and twisting towards micromachined structures which are no longer constrained by the silicon substrate underneath after undercutting, as illustrated in figure 1. The deformation of micromachined structures can be used to determine the residual stresses of thin films [1–3]. The residual stresses can also be exploited to fabricate mechanical structures with desired configurations, especially the structures with out-of-plane deformation. A real three-dimensional structure can therefore be fabricated through the micromachining technology. The applications of this approach are the predeformed microvalve plates in microfluidic systems [4].

Microcantilevers and microbridges (or in terms of clamped–clamped beams) shown in figure 1 are two fundamental predeformed mechanical structures. In general, the bending effect predeforms the cantilever, which contains one fixed end and one free end, as indicated in figure 1(a). On the other hand, the buckling effect predeforms the microbridge, which contains two fixed ends, as indicated in figure 1(b). The mechanical behaviors of cantilevers have recently been studied extensively [5, 6] and well understood; however, the information regarding the buckling behavior of micromachined structures is still limited [7–9]. This is mainly due to the difficulties of predicting the elastic instability phenomena of the buckling behavior. For instance,

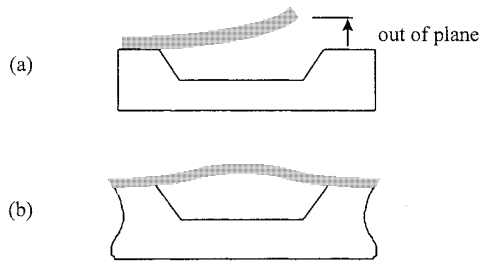

Figure 1. Out-of-plane deformation of: (a) microcantilever; and (b) microbridge.

the buckling of a microbridge could be affected by thin film residual stresses, fabrication processes, as well as boundary conditions. In fact, most of the models still considered the buckling behavior as a linear perfect case [8, 9]. Though the imperfection effect during buckling was mentioned in [7], the sources that may introduce imperfections were not discussed. The applications of predeformed microbridges are thus limited.

The goal of this research is to develop a model regarding the imperfections of a microbridge during buckling. The unsymmetric and flexible boundaries of the microbridges and the gradient residual stress are considered as two major sources of imperfections in the proposed approach. The buckling behavior of the microbridges observed in the experiment can be explained qualitatively by using a study of the boundary and residual stress.

0960-1317/99/030236+09$30.00

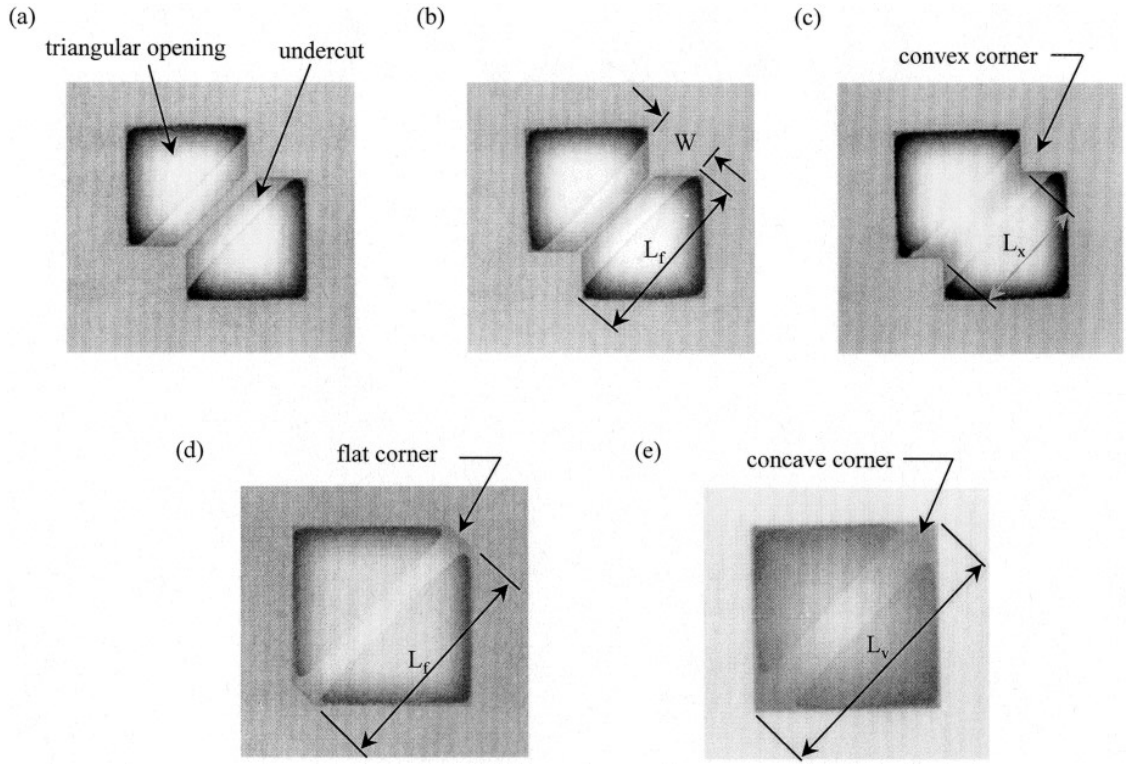

Figure 2. Fabrication of a microbridge: (a) not fully undercut; (b) not fully undercut; (c) fully undercut with convex corner boundaries; (d) fully undercut with flat boundaries; and (e) fully undercut with concave corner boundaries.

2. Experiment and results

In order to observe the buckling behavior of microbridges, SiO_2 beams of various lengths and thicknesses were fabricated using a standard bulk micromachining process. A SiO_2 layer was thermally grown at 1050 °C on a (100) single-crystal silicon substrate. After the SiO_2 layer was patterned using hydrofluoric acid, the wafer was etched anisotropically with a 25% KOH solution at 80 °C. The SiO_2 beams were suspended above a cavity after the silicon substrate underneath was removed.

The etching time must be controlled properly so as to obtain the desired boundaries of the beams. The optical microscope photographs in figure 2 show an undercut process of a silicon substrate for SiO_2 microbridge patterns. The triangular openings indicated in figure 2(a) were apt to form two pyramid cavities on its underlying silicon substrate after anisotropic etching [10]. As shown in figure 2(b), the width of the microbridge was W, and the hypotenuse of the triangular openings was L_f. When the microbridge was just released from the substrate, two convex corners formed its boundaries, as indicated in figure 2(c). The effective length of the microbridge L_x, as indicated in figure 2(c), hence was approximately equal to $L_f - W/2$. The convex corner became flat for a longer etching time, as shown in figure 2(d). The undercutting process was stopped by (111) planes; therefore, two concave corners were formed on the silicon substrate, as indicated in figure 2(e). The effective length of the microbridge became L_v $(= L_f + W/2)$ under this circumstance. Thin films with thicknesses between 0.3 and 1.0 μm were grown in the experiment; arrays of microbridges with a length L_f between 30 and 120 μm were also fabricated. Since the length L_f and the thickness h of the microbridges were two key factors studied in this research, these samples were tested during the experiment.

The buckling amplitude orientation of each microbridge was characterized by both an optical microscope and interferometric profilometry. The microbridges were confirmed from observed results to buckle with their amplitude either upward or downward. Deflection measurements for microbridges of thirty different lengths and from twenty different arrays on the same wafer demonstrated the variations of the buckling amplitude orientations (upward or downward) with length for W and h specified. Typical measured results for the microbridges with concave corners and flat boundaries are indicated in figures 3 and 4, respectively. The data bars in figures 3 and 4 denote the percentage of the buckling amplitude orientations for a specific beam length of a microbridge. The positive and negative y-axis in figures 3 and 4 represent the upward and downward directions, respectively.

Shorter microbridges are clearly found as tending to buckle downward, according to the measurements, whereas longer microbridges tend to buckle upward. Between the two regions of different buckling amplitude orientations, there is a transition region, for example 38 to 42 μm in length for a 0.67 μm thick microbridge as shown in figure 3(a). The transition region of a thicker microbridge occurs in a beam of longer length. For instance, the transition region ranges from 46 to 50 μm in length for a 0.85 μm thick microbridge as shown in figure 3(b). For the case of 1 μm thick microbridges, it is difficult to distinguish from figures 3(c)

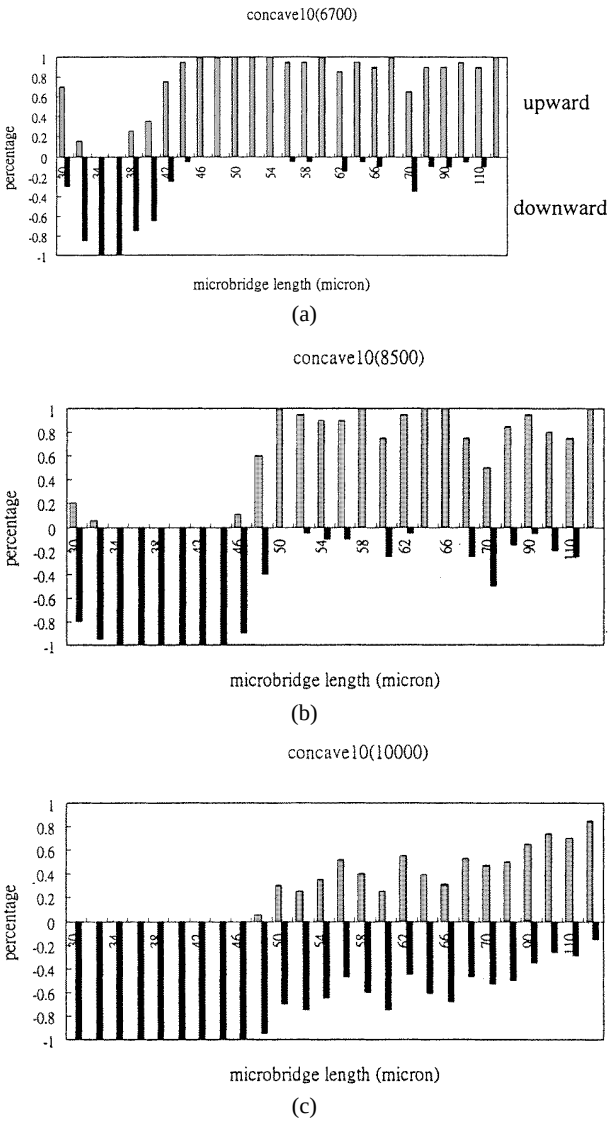

Figure 3. Variation of the buckling amplitude orientations (as a percentage) with length for a microbridge with various thicknesses: (a) 0.67 μm; (b) 0.85 μm; and (c) 1.0 μm. The boundaries of the microbridge are concave corners. Measurement results for each beam length are taken from 20 different beams.

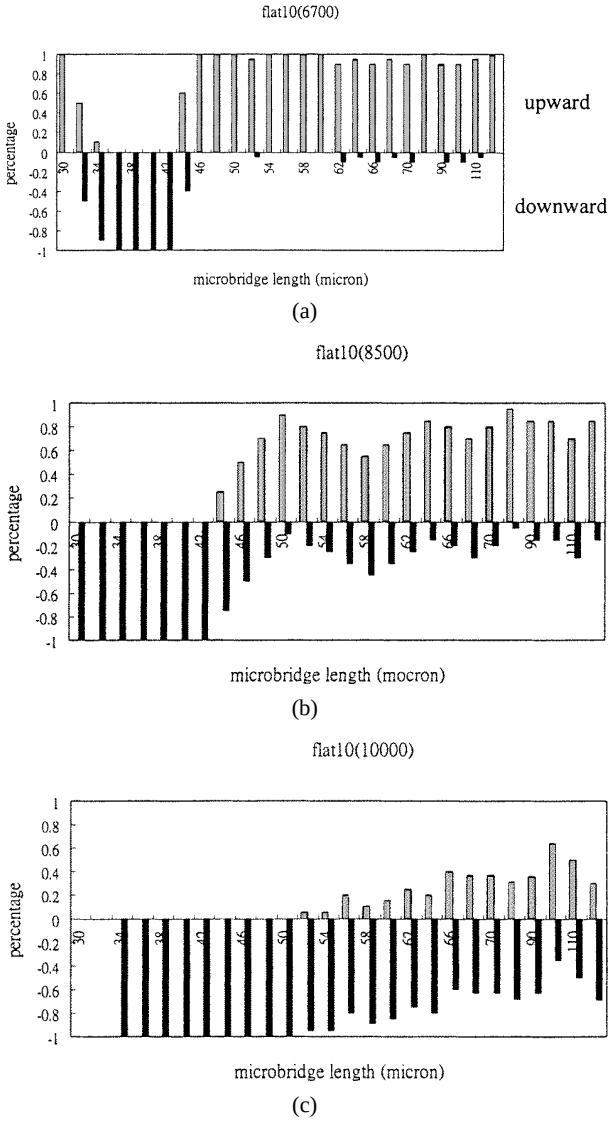

Figure 4. Variation of the buckling amplitude orientations (as a percentage) with length for a microbridge with various thicknesses: (a) 0.67 μm; (b) 0.85 μm and (c) 1.0 μm. The boundaries of the microbridge are flat edges. Measurement results for each beam length are taken from 20 different beams.

and 4(c) whether their beam lengths reached the transition region. The microbridge still tends to buckle upward while the length increases, as indicated in figure 3(c). Though the boundaries of the microbridges in figures 3 and 4 are different, their measured results have the same trends. In short, the buckling amplitude orientations of microbridges with various beam lengths are confirmed from the measured experimental results not to be distributed randomly.

3. Modelling and analysis

A general residual stress σ in a thin film can be expressed using the polynomial [1]

$$\sigma = \sum_{0}^{\infty} \sigma_k \left(\frac{2y}{h}\right)^k \tag{1}$$

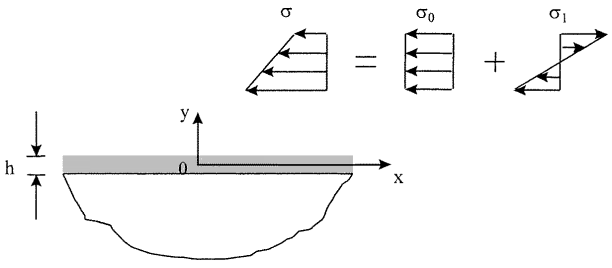

Figure 5. Thin film residual stress with uniform and gradient components.

where h is the thickness of the thin film. The origin of the coordinates is chosen at the film's mid-plane, thus $y \in (-h/2, h/2)$, as illustrated in figure 5. In the first approximation, the residual stress is regarded as the superposition of a uniform component σ_0 and a gradient

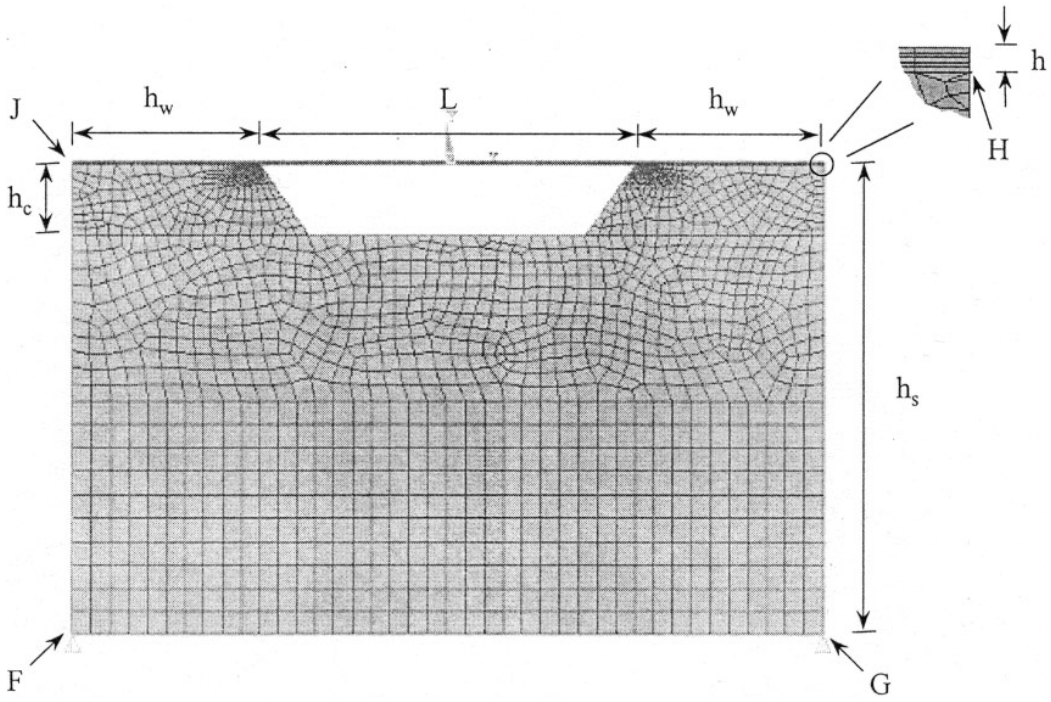

Figure 6. A two-dimensional model of a microbridge with length L and thickness h.

component $\sigma_1(2y/h)$ (or called σ_1). The beam with its two ends fixed will buckle if the compressive force exerted on the beam is greater than the critical buckling load P_c [11]

$$P_c = \frac{4\pi^2 EI}{L^2} \tag{2}$$

where L and EI respectively represent the length and flexural rigidity of the beam. It may be deduced from (2) that a microbridge will buckle if its uniform residual stress reaches a critical value σ_c.

If the beam was a perfect structure (idealization of geometry and loading), it would have an equal opportunity to buckle upward and downward. On the contrary, if the beam had imperfections, it would tend to buckle towards a specific direction [12]. There are several possible sources, including fabrication defects, geometric irregularities, non-ideal loadings and boundaries, which introduce imperfections into microbridges. The buckling amplitude orientations of the microbridges observed in this experiment were found to be strongly dominated by these imperfections. It is believed that this is the main reason for the regular distribution of the buckling amplitude orientations of microbridges as shown in figures 3 and 4.

It is important to predict the buckling amplitude orientations of microbridges at the design stage in order to apply the characteristic of a buckling beam to a microsystem. The buckling behavior associated with the geometrical shape (including length and thickness) and the imperfections of microbridges are discussed in this study. The sources of imperfection include the boundaries of the microbridge and the gradient residual stresses of thin films. Commercial software was used to establish finite element models with which to explain the buckling behavior observed in the experiment. To clarify the influence of the geometrical

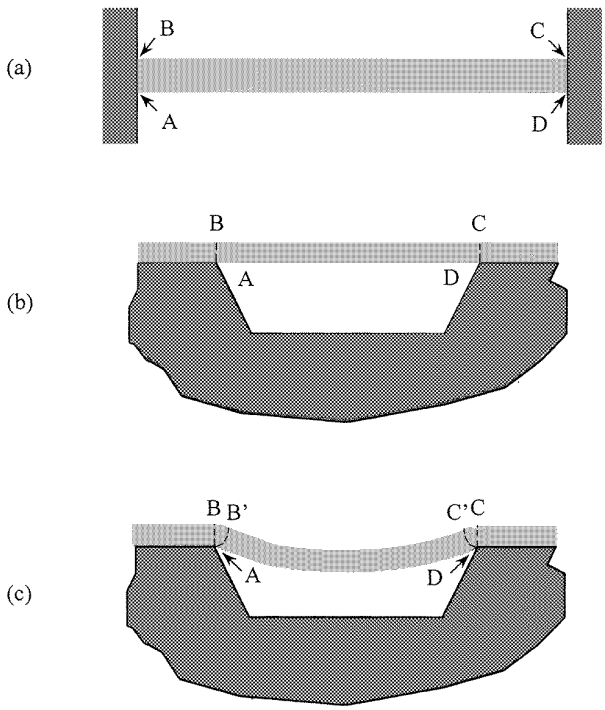

Figure 7. The side-view of a microbridge: (a) for a conventional boundary AB; (b) for a proposed boundary AB; and (c) the boundary AB before the relief of σ_0; and the boundary AB′ after the relief of σ_0.

shapes and the imperfections on the buckling behavior of microbridges, the model was carried out using the nonlinear analysis. A simple two-dimensional finite element model, including a microbridge and its underlying silicon substrate, established in this study is shown in figure 6. The model

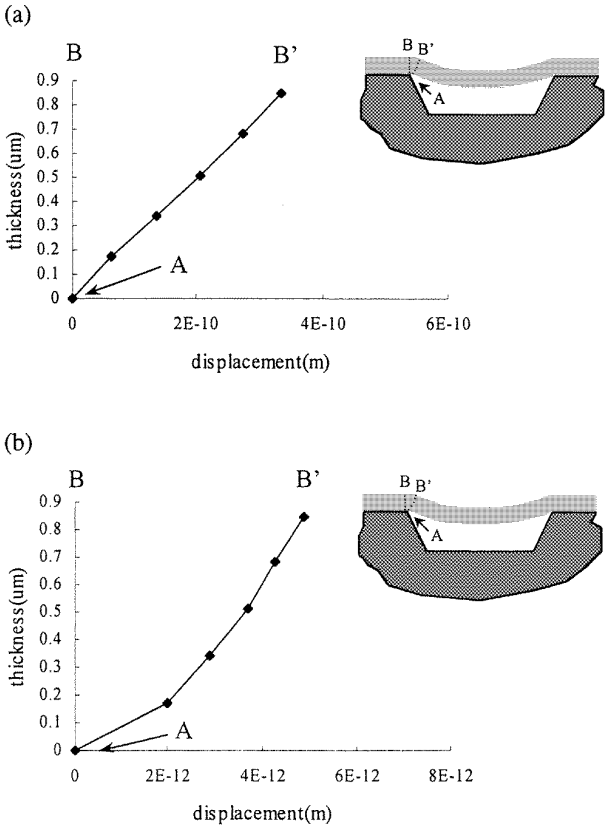

Figure 8. The change of the boundaries AB of these models with lengths: (a) 36 μm; and (b) 100 μm. These models were only subjected to uniform residual stress. Line AB represents the undeformed left boundary, whereas line AB′ represents the boundary configuration of the microbridge subjected to uniform stress at the prebuckling state.

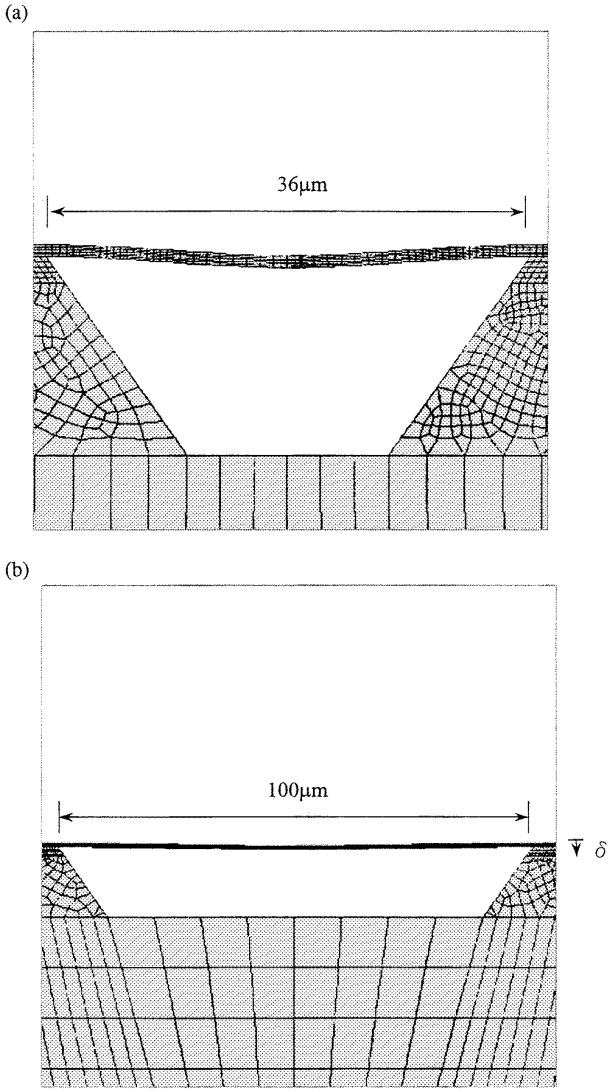

Figure 9. Prebuckling shapes of the simulated (a) 36 μm and (b) 100 μm long microbridges only subjected to uniform residual stress.

represents the cross section of a microbridge along its axial direction. The domain FGHJ indicated in figure 6 represents the silicon substrate. In addition, L represents the length of the microbridge; h_s is the thickness of the silicon substrate; h_c is the depth of the cavity when the microbridge is just released from the underlying silicon substrate. The boundary conditions of the model were applied at points F and G by means of constraining their displacement in the y direction; however, the rest of the region of the model is free to expand and bend.

In this study, the material used for the microbridges was thermal SiO_2 with residual stress $\sigma_0 = -300$ MPa. The finite element models with the same film thickness, $h = 8500$ Å, and six different lengths $L = 36\ \mu$m, $50\ \mu$m, $55\ \mu$m, $60\ \mu$m, $80\ \mu$m and $100\ \mu$m, respectively, were established. The models represent different buckling amplitude orientations due to different lengths shown in figures 3(b) and 4(b). The silicon substrate used in the experiment was 500 μm thick. The elastic moduli of SiO_2 and Si were respectively taken to be 70 GPa and 190 GPa [13], and the Poisson's ratios of SiO_2 and Si were assumed to be 0.15. The thickness of the substrate h_s, as was indicated from a nonlinear analysis, would not influence the results of the finite element analysis while h_s exceeds 300 μm. The thickness h_s in the finite element model therefore was only 300 μm instead of 500 μm so as to save computational time. Similarly the wall thickness h_w was modelled to be 50 μm but not several millimetres.

3.1. Boundary effect

The conventional fixed (or clamped) condition has zero displacement and zero slope along the boundary, as is illustrated in figure 7(a). The boundary conditions of micromachined structures however, are limited to the fabrication processes. The boundary conditions of a microbridge shown in figure 7(b) are different from those of the conventional clamped–clamped beam indicated in figure 7(a). The boundaries AB and CD of a microbridge depicted by the broken lines in figure 7(b) are only fixed at points A and D. Thus, AB and CD would expand to the broken lines AB′ and CD′ shown in figure 7(c) after the relief of a uniform compressive residual stress. The microbridge consequently is bent to form the configuration shown in figure 7(c) due to its deformed boundaries.

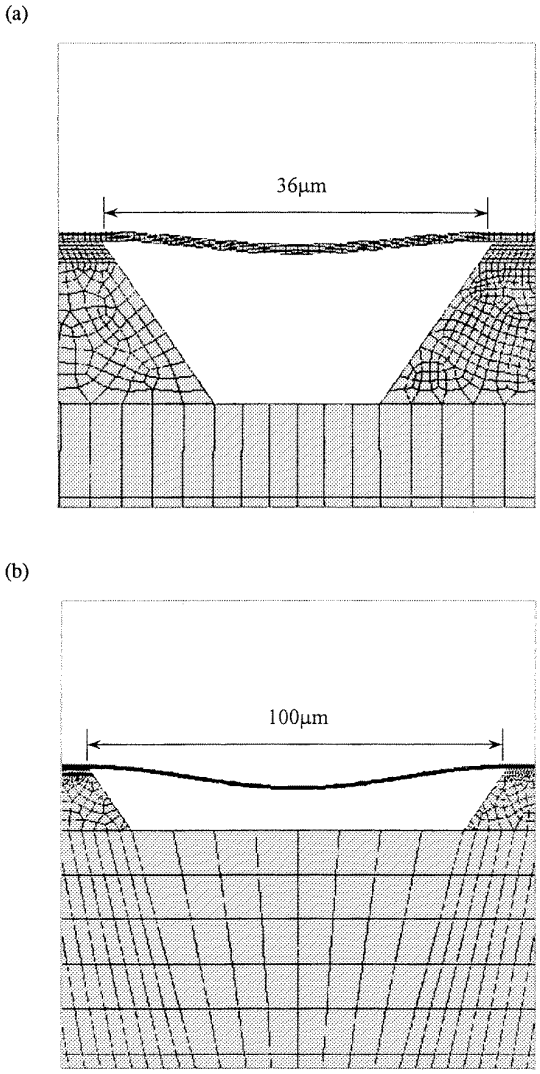

Figure 10. Postbuckling shapes of the simulated (a) 36 μm and (b) 100 μm long microbridges only subjected to uniform residual stress.

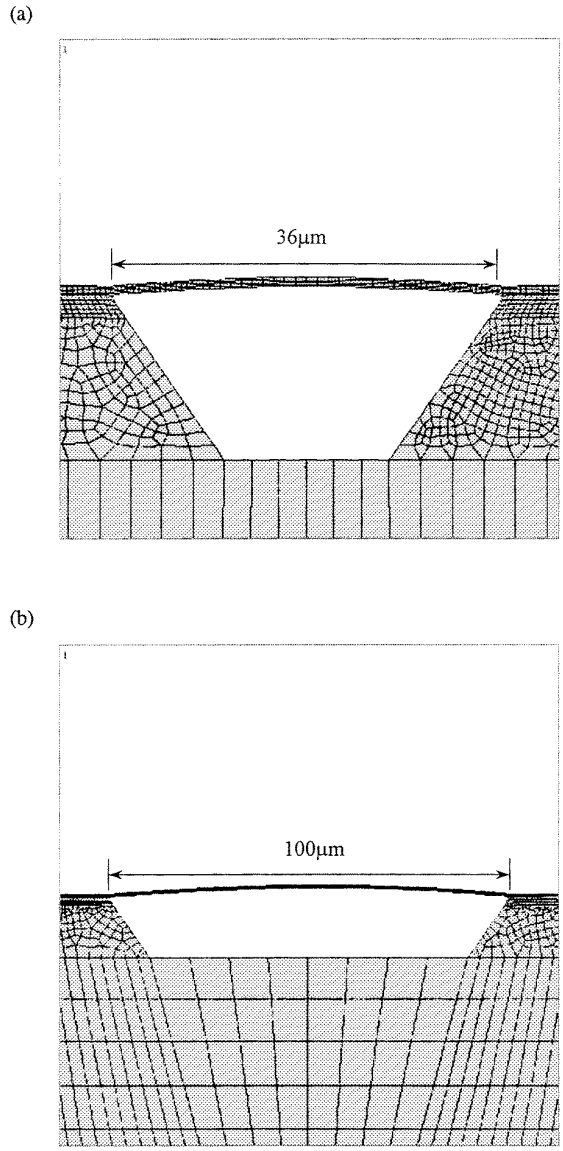

Figure 11. Deformed shapes of the (a) 36 μm and (b) 100 μm long microbridges after being subjected to gradient residual stress only.

In order to clarify the influence of the boundary effect on the buckling behavior by means of finite element analysis, the model shown in figure 6 was subjected to a uniform residual stress. The boundary AB of the microbridge with arbitrary beam length was deformed to a similar configuration, as was indicated from a nonlinear analysis. Two typical deformed boundary configurations AB′ for microbridges with L = 36 μm and 100 μm are shown in figure 8. Microbridges with arbitrary beam length were clearly indicated from previous analysis to have the initial configuration shown in figure 9 at their prebuckling state. Since buckling amplitude orientation was very sensitive to the initial configuration of the beams at their prebuckling state, the microbridges were all buckled downward. For instance, the buckling of microbridge with L = 36 μm and 100 μm are shown in figure 10. To summarize, the boundary of a microbridge is a source of imperfection leading the microbridge to buckle downward.

3.2. Bending effect

Gradient residual stresses would result in the bending of a microbeam as shown in figure 1(a), after the underlying silicon substrate was removed [1, 6]. In this regard, a microbridge should be no longer a perfect straight beam while it is subjected to σ_1 described in equation (1). The deformation profile of a microbridge induced by gradient residual stresses hence would affect the buckling amplitude orientations. Microbridges influenced by gradient stresses were analysed using the finite element model shown in figure 6.

In the present finite element model, 0.85 μm thick SiO_2 microbridges with six different lengths were studied. The gradient residual stress σ_1 of a 0.85 μm thick SiO_2 film determined from the curvature of a micromachined cantilever was 6.25 MPa. Two typical simulated shapes of the 36 μm and 100 μm long microbridges, under the action of the

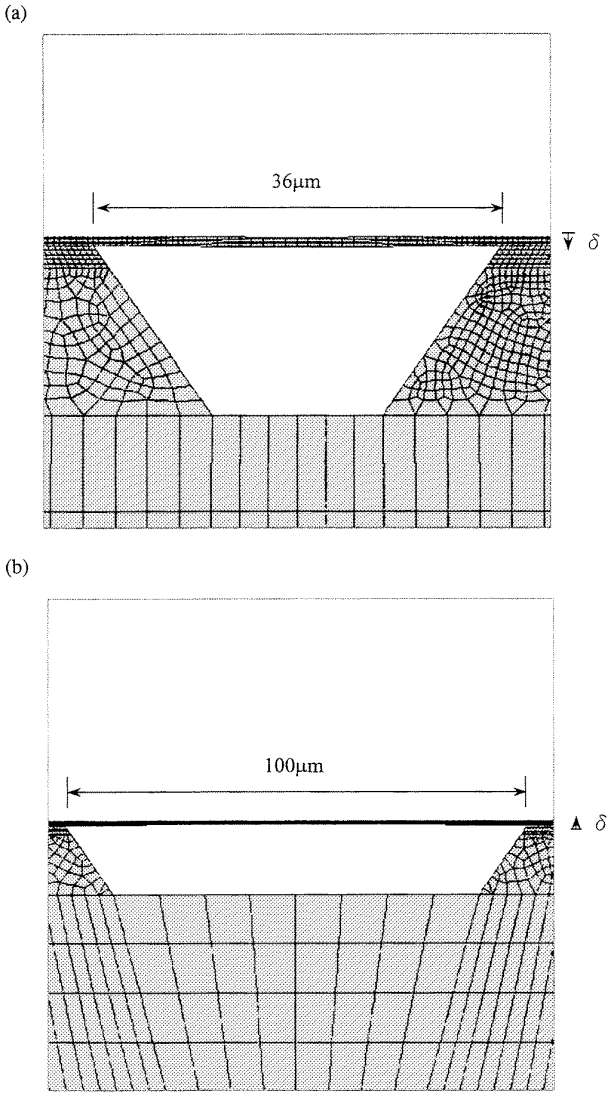

Figure 12. Prebuckling shapes of the simulated (a) 36 μm and (b) 100 μm long microbridges subjected to both uniform stress and gradient stress.

gradient residual stress σ_1, were consequently both bent upward, as illustrated in figure 11. In short, the initial configuration induced by the gradient residual stress of the SiO_2 film in the studied case tends to induce microbridges to buckle upward.

3.3. Net effect

Residual stresses of thin films consist of both the uniform σ_0 and the gradient σ_1 components. The initial configuration of a microbridge at the prebuckling state is thus determined by both the boundary effect and the bending effect. The σ_0 and σ_1 values were imposed on the models by means of finite element analysis. The initial configuration of the microbridges with lengths $L = 36\,\mu$m and 100 μm are shown in figure 12. The initial configuration of the 36 μm long microbridge remained deflecting downward after imposing the bending effect, as is indicated from a comparison of figure 9(a) with figure 12(a). On the contrary, the initial

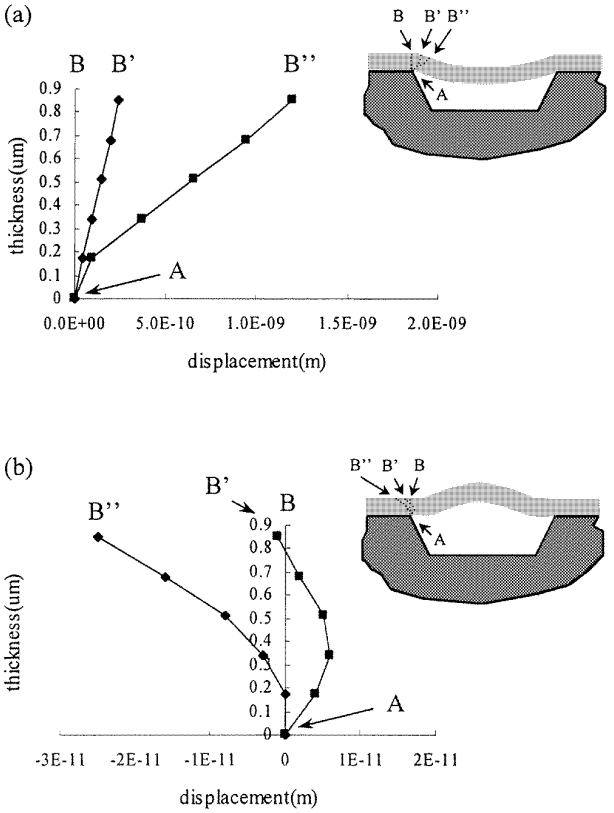

Figure 13. The change of boundaries AB for the models with lengths of (a) 36 μm and (b) 100 μm. These models were subjected to uniform stress and gradient stress. Line AB represents the undeformed left boundary of the microbridge. Line AB′ represents the boundary configuration of the microbridge at the prebuckling state, whereas line AB″ represents the boundary configuration of the microbridge at the postbuckling state.

configuration of the 100 μm long microbridge shown in figure 12(b) became deflected upward after imposing the bending effect. The boundary of the microbridge changed from the initial state AB to the prebuckling state AB′ as shown in figure 13. The 36 μm long microbridge therefore remained buckled downward, whereas the 100 μm long microbridge became buckled upward, as illustrated in figure 14. The boundary of the microbridge at the postbuckling state AB″ is also indicated in figure 13.

The variations of the buckling amplitude orientations for six different lengths of the microbridge were also studied using the finite element model, as shown in figure 15(a). The microbridges were demonstrated from the analysis to buckle downward while $L = 36\ \mu$m, 50 μm and 55 μm, and buckle upward while $L \geqslant 60\ \mu$m. The transition length was near 50 μm to distinguish the buckling-up region from the buckling-down region of the microbridges, as was illustrated from a comparison of the simulated results with the experimental results shown in figures 3(b) and 4(b). As another example, the 0.67 μm thick SiO_2 microbridges with five different lengths were also studied by means of the finite element model. The distribution of the buckling amplitude orientations with the beam lengths is shown in figure 15(b). The microbridges were demonstrated from the analysis to buckle downward while $L = 30\ \mu$m and 35 μm, and buckle

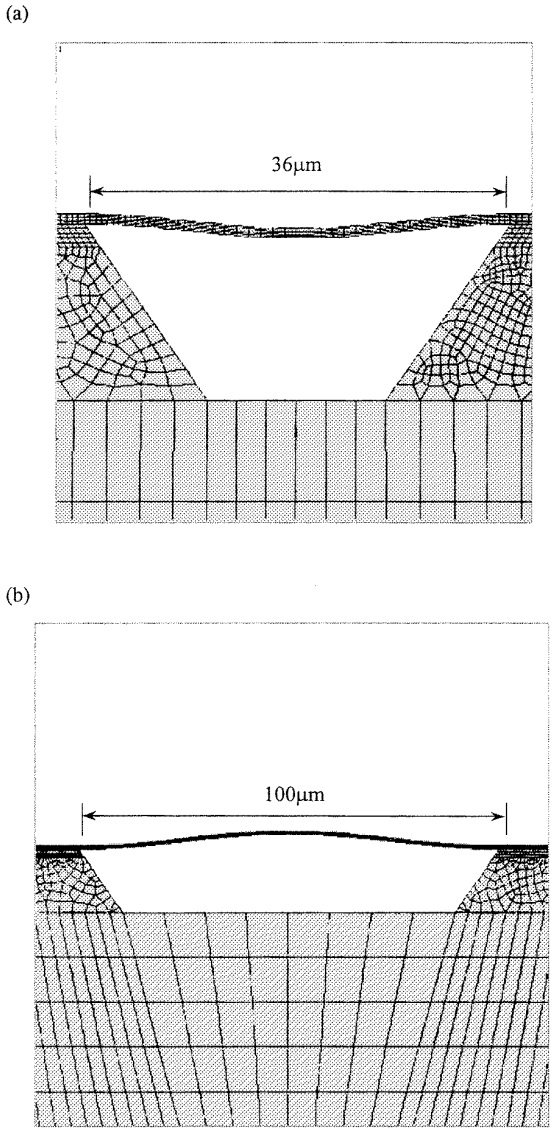

Figure 14. Postbuckling shapes of the simulated (a) 36 μm and (b) 100 μm long microbridges subjected to both uniform stress and gradient stress.

upward while $L \geqslant 40$ μm. The transition length of the microbridge obtained through the experiment, however, was near 44 μm, as indicated in figures 3(b) and 4(b).

4. Discussion and conclusion

The buckling amplitude orientation of a microbridge is influenced substantially by its initial configuration. In this study, two primary imperfection sources, which may produce the initial configuration of a microbridge, were demonstrated using finite element models. The first imperfection source is the deformation of the partially clamped boundaries AB and CD for a microbridge shown in figure 7(b). The partially clamped boundaries may thus introduce an angular deflection θ at the boundaries of the microbridge. The initial configuration of the microbridge induced by this effect is regarded as the model shown in figure 16(a). In this case, the microbridge is considered to be bent by an effective bending

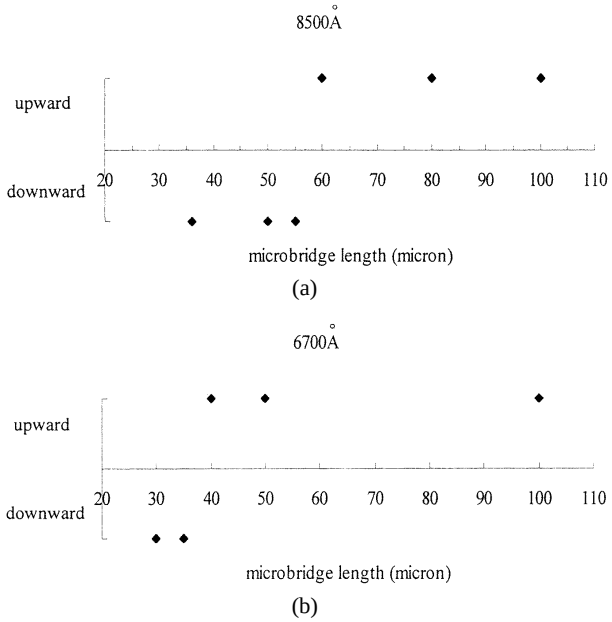

Figure 15. Simulated results of the variation of the buckling amplitude orientations with length for microbridge with two different thicknesses: (a) 0.85 μm and (b) 0.67 μm.

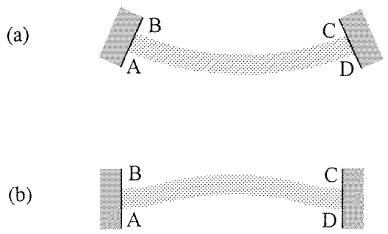

Figure 16. The influence of: (a) boundary effect; and (b) bending effect on the configuration of a microbridge.

moment

$$M_0 = \frac{2EI\theta}{L} = \frac{Ebh^3\theta}{6L}. \tag{3}$$

In short, the boundary effect, as indicated in figure 16(a), is an imperfection leading the microbridges to buckle downward. The second imperfection source is the bending of the microbridge due to the gradient residual stress σ_1 of thin films. The initial configuration of the microbridge induced by this effect is regarded as the model shown in figure 16(b). In this case, the microbridge is bent by a bending moment

$$M_1 = \frac{2I\sigma_1}{h} = \frac{bh^2\sigma_1}{6}. \tag{4}$$

The gradient stress of the SiO_2 film resulting in the bending of a microbridge, as indicated in figure 16(b), is an imperfection leading it to buckle upward.

The effective moment M_0 is found from (3) to decrease while the microbridge length L increases, whereas the moment M_1 is found from (4) to remain a constant while L changes. In general, M_0 would dominate the buckling amplitude orientations for shorter microbridges. On the other hand, M_1 would dominate the buckling amplitude orientations for longer microbridges. In addition, M_0 is proportional to h^3; however, M_1 is proportional to h^2. The

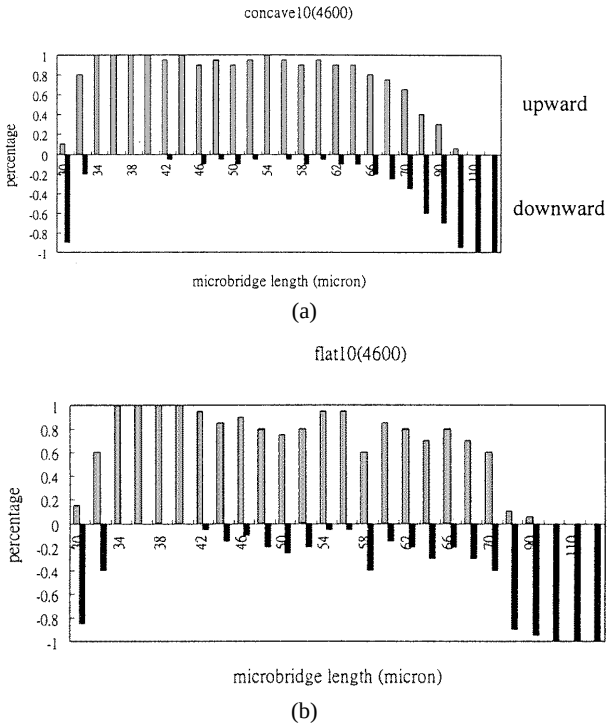

Figure 17. Variation of the buckling amplitude orientations (as a percentage) with length for 0.46 μm thick microbridge. The boundaries of the microbridge respectively are: (a) concave corners; and (b) flat edges. Measurement results for each beam length are taken from 20 different beams.

microbridge therefore tends to widen its buckling-down range corresponding to the increase of the film thickness. This is the explanation for the experimental observations shown in figures 3 and 4. According to (3) and (4), the buckling amplitude orientation of a microbridge can be estimated or controlled if the proper film thickness, beam length and thin film residual stresses are chosen.

The buckling amplitude orientations of 0.85 μm thick microbridges with various lengths were simulated. Microbridges shorter than 55 μm consequently buckled downward, whereas the microbridges longer than 60 μm buckled upward, as indicated from the simulated results of figure 15. The change in the buckling amplitude orientation is indicated from the simulation to occur between 55 and 60 μm long microbridges. Compared with experimental results, there is a shift of 5–10 μm in the transition region. There is also a 5–10 μm difference in the transition region between the experimental and analytical results for 0.67 μm thick microbridges; this may be because the model took no account of the boundary effects introduced by the real shapes of the convex and concave corners shown in figure 2. In addition, the gradient residual stresses of the 0.67 μm thick and 0.85 μm thick thin films were obtained using interpolation. This approach may be another possibility by which to induce the deviation to the distribution of the transition region compared to the experimental results.

The thinner microbridges all buckled downward when their lengths L became larger, as indicated in figure 17. The 0.46 μm thick microbridges however were apt to buckle downward again after their lengths exceeded 70 μm. Almost all of the microbridges additionally buckled downward for all lengths when their thickness was only 0.3 μm. This characteristic is believed to be introduced by surface tension from de-ionized water during drying the wafer. For the case of thinner microbridges, their stiffness is too small to tolerate the absorption of surface tension; thus, the buckled microbridge would experience a snap through a deflection from the upward position to the downward position.

Acknowledgments

This material is based (in part) upon work supported by the Precision Instrument Development Center and the National Science Council under Grant NSC 87-2218-E007-007. The author would like to thank the Electrical Engineering Department of the National Tsing Hua University, Semiconductor Center of National Chiao Tung University and the National Nano Device Laboratory for providing the fabrication facilities. The authors would also like to thank Professor R S Huang for his valuable suggestions.

References

[1] Fang W and Wickert J A 1996 Determining mean and gradient residual stresses in thin films using micromachined cantilevers *J. Micromech. Microeng.* **6** 301–9

[2] Mehregany M, Howe R T and Senturia S D 1987 Novel microstructures for the *in situ* measurement of mechanical properties of thin films *J. Appl. Phys.* **62** 3579–84

[3] Guckel H, Burns D, Rutigliano C, Lvell E and Choi B 1992 Diagnostic microstructures for the measurement of intrinsic strain in thin films *J. Micromech. Microeng.* **2** 86–95

[4] Haji-Babaei J, Kwow C Y and Huang R-S 1997 Integratable active microvalve with surface micromachined curved-up actuator *Int. Conf. Solid-State Sensors and Actuators (Chicago, IL, June, 1997)* pp 833–6

[5] Chen Y 1997 The fabrication and discussion of silicon nitride membranes by chemical vapor deposition *Master Thesis* National Chiao Tung University, Taiwan

[6] Chu W-H and Mehregany M 1993 A study of residual stress distribution through the thickness of p^+ silicon film *IEEE Trans. Electron Dev.* **40** 1245–50

[7] Fang W and Wickert J A 1994 Postbuckling of micromachined beams *J. Micromech. Microeng.* **4** 116–22

[8] Guckel H, Randazzo T and Burns D W 1985 A simple technique for the determination of mechanical strain in thin films with application to polysilicon *J. Appl. Phys.* **57** 1671–5

[9] Wilmsen C W, Thompson E G and Meissner G H 1972 Buckling of thermally-grown SiO_2 thin films *IEEE Trans. Electron Dev.* **19** 122

[10] Pugacz-Muraszkiewicz I J 1972 Detection of discontinuities in passivating layers on silicon by NaOH anisotropic etch *IBM J. Res. Dev.* **16** 523–9

[11] Beer F P and Johnson E R Jr 1981 *Mechanics of Materials* (New York: McGraw-Hill)

[12] Dym C L 1974 *Stability Theory and Its Applications to Structural Mechanics* (Leyden: Noordhoff)

[13] Gardner J W 1994 *Microsensors* (Chichester: Wiley)